SPACE-BASED PHOTOMETRIC OBSERVATIONS OF THE SPACEX STARLINK CONSTELLATION SATELLITES – PRELIMINARY FINDINGS

Chance Johnson (a), Dr. Lauchie Scott (b), Stefan Thorsteinson (c)

a. *Defence R&D Canada Ottawa, Ottawa, ON, chance.johnson@drdc-rddc.gc.ca*
b. *Defence R&D Canada Ottawa, Ottawa, ON, robert.scott@drdc-rddc.gc.ca*
c. *Defence R&D Canada Ottawa, Ottawa, ON, stefan.thorsteinson@drdc-rddc.gc.ca*

ABSTRACT

As of 18 October 2020, SpaceX has deployed 835 satellites over 14 launches as part of their proposed internet broadband constellation, known as *Starlink*. The first 60 Starlink satellites, launched in May 2019, caused an unexpected stir in the astronomical community when the orbiting train of satellites were observed, naked eye, by ground-based observers. Their noticeable brightness was attributed to a Starlink satellites' highly reflective surface finishes and their relatively low orbital altitude upon initial deployment. Responding to growing concern by the international astronomy community that a Starlink mega-constellation would obstruct space observations, SpaceX implemented a few different methods to reduce the satellites' brightness. These methods included a darkening finish applied to the bus designed to reduce its reflectivity, a built-in, deployable visor designed to reduce the amount of sunlight incident on the reflective bus surfaces, and actively modifying satellite orientation of the solar panels during orbit raising meant to minimize sunlight reflection.

This paper describes space-based photometric observations of the Starlink satellites collected by Canada's *Near Earth Object Surveillance Satellite (*NEOSSat*)*. These photometric measurements characterize the Starlink constellation from an orbital, rather than ground-based perspective. These findings compliment ground-based measurements of Starlink satellites' brightness which tend to observe the satellites at relatively high solar phase angles. A space-based observer can measure a Starlink satellites' brightness over a variety of solar phase angles adding unique illumination and observer perspective to this constellation's visual footprint on the celestial sphere.

INTRODUCTION

Shortly after the launch of the first batch of 60 Starlink satellites, ground-based visual observers promptly reported the unusual appearance of bright trains of objects moving across the night sky (Fig. 1) [1].
Although Low Earth Orbit (LEO) satellites are regularly observed by the unaided eye; they tend to go unnoticed by most naked-eye observers due to their sparse separation and relatively dim visual magnitude, $M_v > 5$. The initial deployment of the Starlink constellation, with its tight in-track orbital separation of the Starlink satellites and their relatively reflective surface finishes created an unusual moving asterism against the night sky and provoked immediate apprehension by the astronomical community.

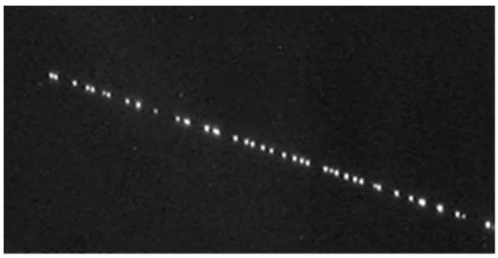

Figure 1. Ground based image of the first 60 Starlink satellites. Langbroek, 2019.

The astronomy community has expressed concern at the broadening industrial expansion in LEO using mega-constellations, where hundreds if not thousands of satellites will be launched into LEO in a manner similar to the Starlink satellite series. Astronomical observers extensively use visible-band detectors for widefield sensing of the celestial sphere to detect potentially hazardous earth orbit crossing asteroids, detect planets orbiting stars in distant solar systems, or for recreational and hobby astronomy. The rapid expansion of LEO constellation infrastructure puts at risk the effectiveness of survey-style astronomical imaging due to potential blemishes created from the streaking of thousands of space objects across images.

Furthermore, the Space Domain Awareness (SDA) community is facing an expanded orbital custody problem with detecting space objects deployed in mega-constellations. Space surveillance sensors are in short supply relative to the thousands of satellites and debris population currently in orbit. Rapidly increasing the task load of an already limited sensing resource poses a significant challenge to SDA sensor operations.

This paper attempts to gain some insight to mega-constellations from a space-based observer perspective. First, the space-based photometric appearance of the SpaceX satellites is characterized, as observed from the orbiting astronomical observatory *NEOSSat*. These space-based measurements offer a unique and complimentary viewing perspective compared to the ground-based characterizations of the SpaceX Starlink satellites that continue to be collected. In-orbit observations can characterize Starlink satellites at various phase angles spanning a variety of illumination conditions, whereas ground-based observers tend to observe LEO satellites at high phase angles and only seeing the Starlinks' nadir, or earth-pointing, face. This additional characterization can help inform future studies in the susceptibility of space-based observatories to the presence of mega-constellations and assist characterizing mega constellation satellites themselves. Space-based observations of these satellites pose an observing challenge due to the brief orbital encounter characteristics of the constellation. The observing strategies required by a space-based optical sensor to observe a Starlink satellite and the combination of observer and target orbits coupled with the observing platform observing limitations are also discussed. Recommendations for future mega-constellations observations from space-based sensors is also provided.

BACKGROUND

The Starlink constellation is a global internet connectivity service under development by SpaceX LLC. The constellation is designed to provide internet connectivity to terrestrial users by use of bidirectional transmission in Ku and Ka band spectrum using ground terminals and modems in operation with non-geostationary orbit satellites using 12 GHz spectrum. The U.S. Federal Communications Commission licensed Starlink in 2018, and has since then authorized the deployment of 12,000 small satellites. The initial orbital configuration consists of 24 planes with 66 satellites per plane, for a total of 1,584 satellites, inclined at 53.8 degrees operating at 550 kilometres altitude [2].

The Starlink space segment utilizes a relatively unique bus geometry (Fig. 2) offering a compact launch configuration within the Falcon 9 launch fairing. Little has been published on space segment's bus however it is believed to use a nadir-facing antenna array with an articulated linear solar array pointing radially from the Earth. For the purposes of this analysis, the main solar array is estimated to be approximately 10 meters in height, 3 meters wide. The rectangular prismatic-shaped bus, based on publicly available imagery, is presumed to be approximately 3 x 1.25 x 0.1 meters in size.

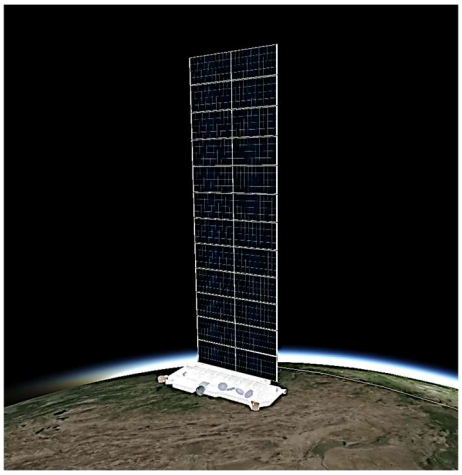

Figure 2. Starlink satellite model showing 10m tall x 3m wide solar array

During the initial deployment of the Starlink satellites, videos from the SpaceX YouTube channel provided the first indications that the satellites were very reflective in their on-orbit configuration. Figure 3 shows frames collected from the deployment of the first 60 Starlink satellites with their solar arrays in their stowed configuration. The second frame shows an apparent glossy-white reflective finish of a Starlink satellite bus while the stack of satellites was slowly separating from one another. The final frame shows the objects beginning to glint from the perspective of the Falcon 9 upper stage camera. These frames suggest a Starlink bus has a significantly reflective finish applied. While these frames do not show the final deployed configuration of these satellites in orbit for the purposes of this analysis, a white finish is assumed to be the reflectance model for bus surfaces with a diffuse albedo of ~90%. The solar array is assumed to have the properties of typical solar cells with a diffuse reflectivity of ~2%.

Figure 3. Starlink launch and deployment. Screen capture from Youtube.com/SpaceX, 2 Sept 2020.

NEOSSAT OBSERVATIONS OF STARLINK CONSTELLATION

NEOSSat and Starlink Observing Geometry

NEOSSat is a 72 kg small space telescope orbiting at 785 km altitude performing on-orbit space surveillance of space objects, asteroids, comets and performs exoplanet astronomy. The microsatellite is jointly operated between the Canadian Department of National Defence and The Canadian Space Agency. *NEOSSat* was launched into orbit in February 2013. The spacecraft's primary payload is a 15 cm on-axis visible light Maksutov telescope fixed to the satellite body. The satellite must slew its body to point the telescope toward space objects. This instrument provides a field of view of 0.8x0.8 degrees^2 using a passively cooled E2V 47-20 Advance Inverted Mode Operation Charge-Coupled Device (CCD) detecting visible wavelengths from 400-900 nm. A separate E2V 47-20 CCD is mounted adjacent to the main science detector and functions as a co-boresighted star tracker enabling fine guidance during tracking of Resident Space Objects (RSOs) and other celestial objects. *NEOSSat's* payload is fitted with a bevelled

cylindrical baffle and serves to suppress off-axis light from the Sun when observing at low solar elongation [3].

Candidate Starlinks for space-based observation are planned using Two-Line Element (TLE) data from Celestrak.com and Systems Tool Kit (STK) software by Analytical Graphics Inc to predict Starlink position in relation to *NEOSSat*. While designed to image deep space objects, *NEOSSat* can track LEO objects during brief windows where all spacecraft imaging constraints and slewing capabilities are met. These windows appear as a Starlink satellite is either rising or setting close to the Earth limb relative to *NEOSSat*. An example accesses window from NEOSSat to several Starlink satellites is shown in Figure 4, where line of sight ranges are maximal (between 1600 and 3000 km) and the relative angular rates minimal (between 50 and 220 arcsec/s). For illustration purposes, only a small subset of the constellation is displayed.

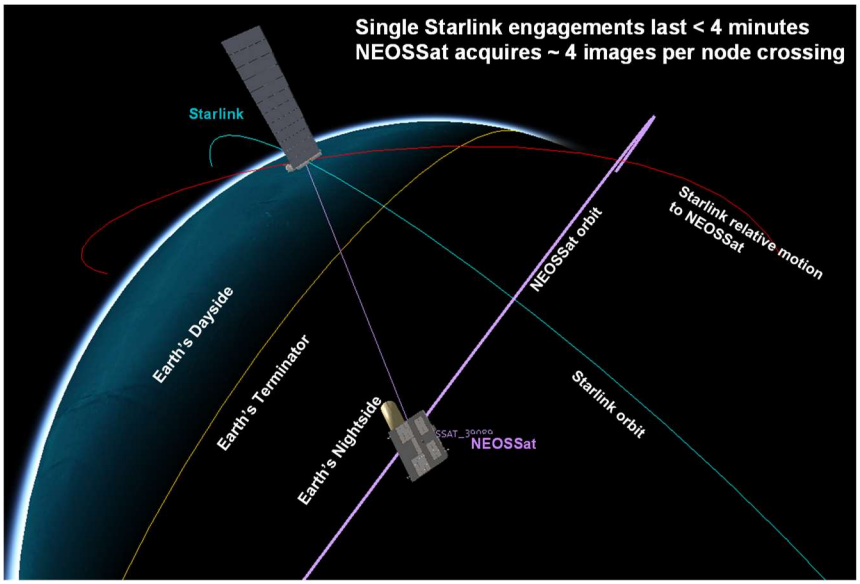

Figure 4. Typical NEOSSat access to Starlink based on constraints.

These constraints lead to two possible windows to observe a Starlink while in line of sight to NEOSSat. An example of these rise and set windows is shown in Figure 5, where observing is not possible at close ranges.

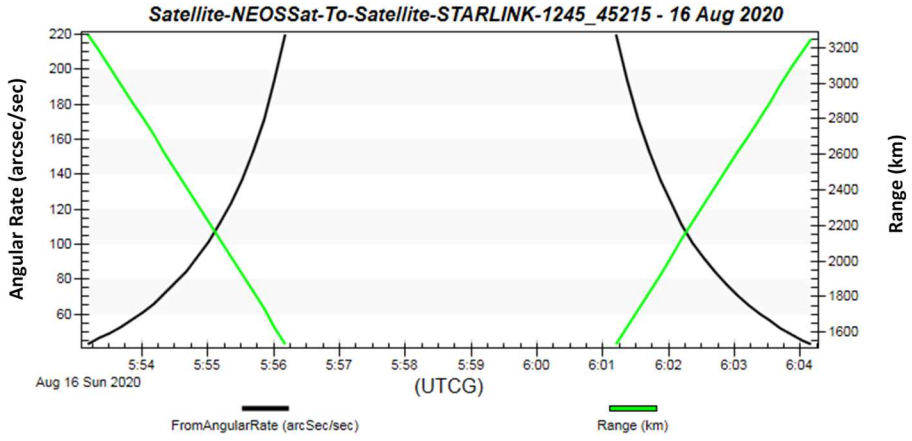

Figure 5. Range and angular rate of a Starlink during accesses when all constraints are met during one pass.

This LEO-to-LEO observing strategy is complicated by the fact that the current Starlink constellation flies at an operational altitude ~200 km lower than *NEOSSat*, and spend the a large portion of their line of sight to *NEOSSat* with the background obscured by the Earth-lit atmosphere.

The following constraints were applied during the planning of *NEOSSat* observation of Starlink satellites:

- *NEOSSat*'s star tracker is not obscured by the Earth during fine slews (i.e. Stars must be continuously present during tracking operations)
- RSO grazing angle above the Earth limb is greater than 10 degrees to avoid atmospheric scattered light and air glow
- *NEOSSat* max angular rate: 220 arcsec/sec
- Solar exclusion angle: 45 degrees
- Lunar exclusion angle: 5 degrees
- RSO is in direct sunlight (i.e. outside of Earth's shadow)
- Minimum temporal access duration between *NEOSSat* and RSO of 90 seconds
- Roll is selected so instrument radiator points (preferentially) toward deep space

NEOSSat acquires imagery at a rate of 1 full frame image every 15 seconds in 2x2 binning. A short exposure of 400 milliseconds was used to help reduce the likelihood that a bright Starlink satellite would saturate *NEOSSat*'s CCD. With this strategy *NEOSSat* collected images in tracks of 4 frames, where *NEOSSat* slews and matches the average relative rate of the Starlink relative to *NEOSSat* over the engagement duration (~75 seconds).

Observation Strategy

The team began *NEOSSat* observations of various Starlink satellites in January 2020. Figure 6 shows a composite of *NEOSSat* imagery acquired during a successful track on a single Starlink. The Starlink is identifiable as a larger, multi-pixel point source near the middle of the frame. Once imagery was downloaded, image processing, including the detected magnitude of the satellite, was performed using an astronomical imaging software program called MaxIm DL™. Photometric measurements were calibrated using a NEOSSat instrumental zeropoint of 21.6 magnitudes/count, which is based on historical *NEOSSat* imagery and Landolt reference star field photometric calibration.

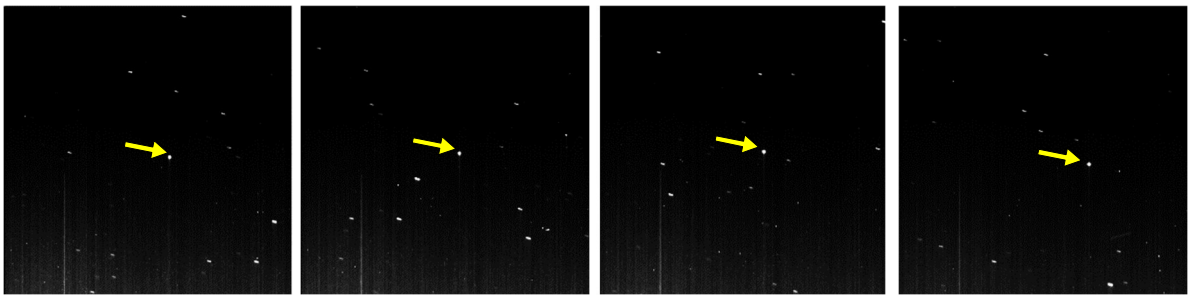

Figure 6. Successful NEOSSat Track (4 images) of a Starlink satellite

Early space-based observation attempts on the Starlink satellites resulted in a relatively low rate of successful acquisition. This was attributed to 3 key factors:

First, *NEOSSat* experienced several slew-rate errors during the "fine slew" tracking phase. This was mainly due to *NEOSSat* attempting to begin tracking "rising" Starlinks near the illuminated Earth limb before the 10-degree grazing angle elevation constraint was met. This limit is required because the background surface brightness exponentially increases closer to Earth, limiting RSO sensitivity and reducing the number of

detectable background guide stars for *NEOSSat's* star tracker. The observing strategy was first modified to observe rising Starlinks at the last possible moment of their access window; however, the observing strategy was eventually modified to only include "setting" Starlinks, resulting in a much higher success rate.

Second, when the fine slew setting was achieved, there were multiple occasions when Starlinks did not appear in the frame as expected. A discrepancy was discovered between the TLE predicted position and actual Starlink reference ephemeris data. Several Starlinks were manoeuvring to either reach their nominal orbit altitude or create proper orbital plane spacing using their electric thrust systems. The observing strategy was then modified to only include Starlinks in a relatively stable orbit, which the team verified by examining the Root Mean Square (RMS) orbit residuals provided by Celestrak.com [4]. It was determined that an RMS value less than 0.3 km was consistent with Starlinks which were not undergoing constant thrust orbit raising and the TLEs were more trustworthy for orbit propagation and tasking *NEOSSat*. Unfortunately, this limited the ability to analyse any active orientation techniques employed to reduce satellite brightness during orbit raising.

Lastly, most failed observations attempts were attributed to unique environmental effects impacting image processing. The two strongest effects were: 1) the South Atlantic Anomaly (SAA) where energetic charged particles impact the NEOSSat imager within the geomagnetic anomaly over South America and 2) the bright Earth limb illuminated by the Sun, especially during NEOSSat's motion over the Antarctic ice sheet during the Antarctic summer [3]. An example for each of these cases can be seen in Figure 7 below.

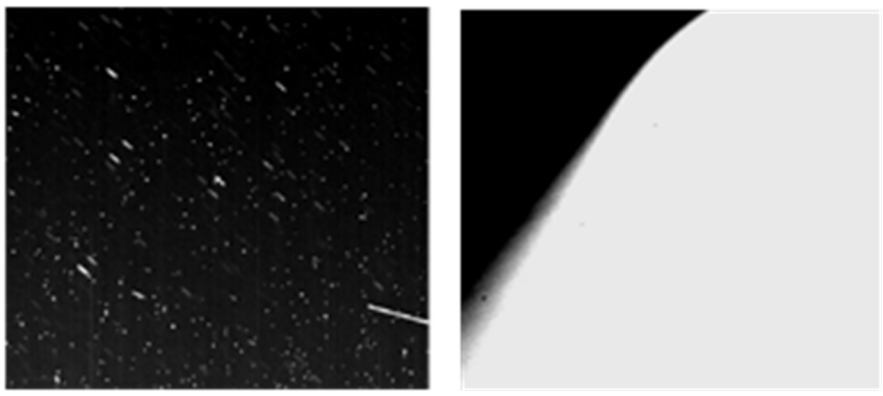

Figure 7. Unsuccessful NEOSSat Tracks of Starlink satellites due to SAA (left) and scattered Earth glow (right).

CHARACTERIZATION / RESULTS

NEOSSat acquired 1494 photometric measurements on 247 unique Starlink satellites (~35% of the constellation), including 32 measurements of Starlink-1130 (also known as "*Darksat*") and 21 measurements of Starlink-1436 (also known as the first "Visorsat") from January 2020 to September 2020.

A portion of this measured population unfortunately did have at least 1 saturated pixel on *NEOSSat's* detector, and this distribution is shown in Figure 8. *NEOSSat* tends to saturate its 2x2 binned pixel array between M_v 8-8.5, with skyglow exacerbating this effect. As the general photometric trend of the objects is preserved, and many unsaturated measurements are interspersed within the saturated set, this photometric analysis uses the full dataset, however it should be recognized that many Starlinks satellites did saturate *NEOSSat*'s detector when observed from orbit.

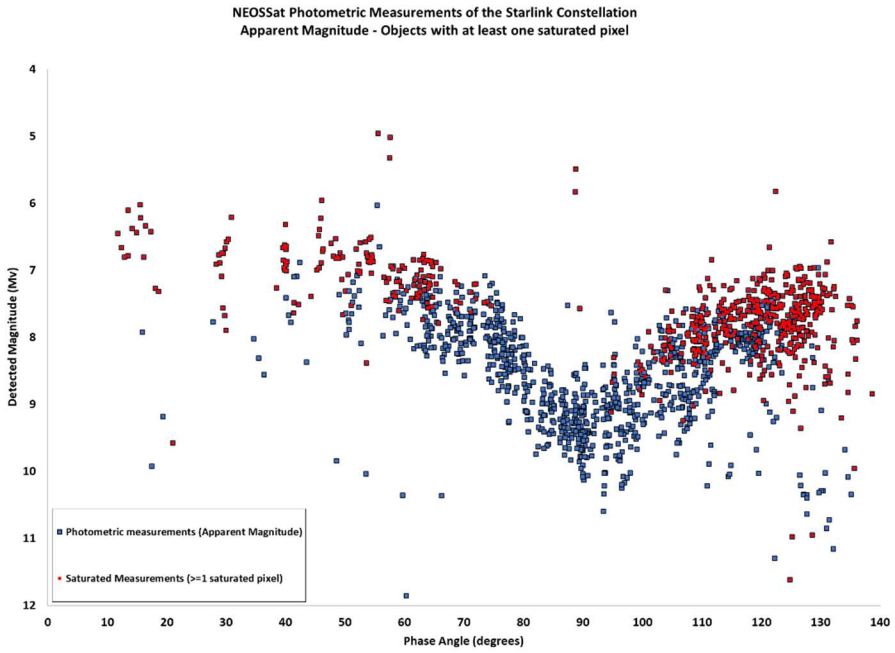

Figure 8: Apparent magnitude of the Starlink constellation vs phase angle. Measurements with at least 1 saturated pixel are overlayed in red.

These photometric measurements were acquired over ranges spanning 1600 to 3000 km from *NEOSSat* to the targeted Starlink. To assist in the development of a photometric model of a specific Starlink's brightness, the detected magnitudes were range normalized to 1000 km using

$$M_{norm} = M_{detected} - 5log_{10}(R/R_0) \quad (1)$$

where R is the range to the Starlink satellite and R_0 is the normalization range. After range normalization, the characteristic magnitudes were plotted against target centric phase angle (Sun/Target/Observer). The range normalized photometric values of the Starlink constellation are shown in Figure 9.

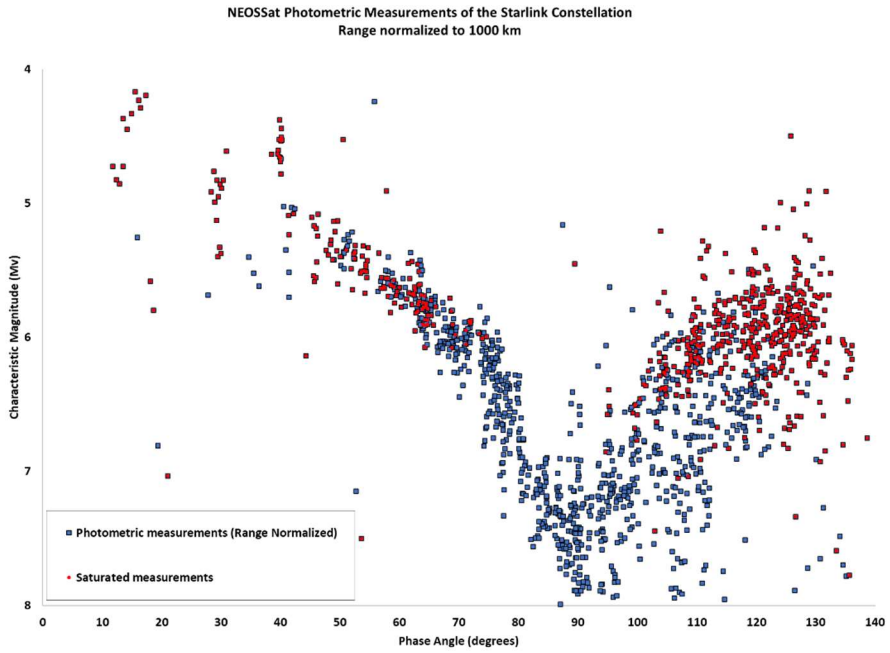

Figure 9: Range normalized photometry of the Starlink constellation vs phase angle

Figure 9 shows two primary areas of photometric behaviour unique to this constellation's "aggregated" light curve. A nightside (antisolar) and dayside observing, and illumination condition produces split behaviour in the constellation's brightness demarcated by 90° phase angle. To further analyse a Starlink's brightness, the photometric data is partitioned into a nightside and dayside model.

Antisolar (nightside) Model: For phase angles (φ) less than 90° (antisolar observations), a Starlink satellite is primarily Sun-illuminated with its main solar panel aligned with the satellite position vector. Assuming that a Starlink's solar panel is Sun-pointing to sustain maximum power generation, a first-order Starlink model using a flat-plate solar panel facet and a spherical bus, as observed by a space-based observer near the Earth's terminator, can be modelled as

$$M_{\varphi<90^\circ} = M_{Sun} - 2.5log_{10}\left(\frac{1}{\pi}\cdot\frac{a_{sp}A_{sp}\langle\hat{\mathbf{n}}\cdot\hat{\mathbf{o}}\rangle\langle\hat{\mathbf{n}}\cdot\hat{\mathbf{s}}\rangle}{R^2}\right) - 2.5log_{10}\left(\frac{1}{\pi}\cdot\frac{a_{bus}A_{bus}F(\varphi)}{R^2}\right)$$

$$\approx M_{Sun} - 2.5log_{10}\left(\frac{1}{\pi}\cdot\frac{a_{sp}A_{sp}\langle\cos(\varphi)\rangle}{R^2}\right) - 2.5log_{10}\left(\frac{1}{\pi}\cdot\frac{a_{bus}A_{bus}F(\varphi)}{R^2}\right) \quad (2)$$

$$\text{as } \langle\hat{\mathbf{n}}\cdot\hat{\mathbf{s}}\rangle \cong 1 \text{ and } \langle\hat{\mathbf{n}}\cdot\hat{\mathbf{o}}\rangle \cong \cos(\varphi)$$

and the phase function $F(\varphi)$ for a sphere is given by

$$F(\varphi) = \frac{2}{3\pi^2}[(\pi - \varphi)\cos(\varphi) + \sin(\varphi)] \quad (3)$$

where M_{Sun} is the magnitude of the Sun (-26.74 magnitudes), a_{sp} is the diffuse albedo of the solar panel, A_{sp} is the cross sectional area of the solar panel, φ is the target centric phase angle, R is the range to the

(1000 km), a_{bus} is the albedo of the spherical bus and A_{bus} is its cross sectional area. The non-negative operator < > returns only positive values or zero from the dot products to model object illumination and visibility on those facets.

A best fit antisolar model to the measured Starlink data is shown in Figure 10. The model uses a solar panel diffuse albedo of ~2% and cross-sectional area of 30 m^2 which is consistent with typical solar panel reflectivity [5] and the estimated cross-sectional area of the Starlink solar panel based on the limited information about Starlink satellites' dimensions. The estimated bus albedo and cross section area are 0.35 and 0.5 m^2, respectively. This simple model does a reasonable job predicting the detected Starlink photometric behaviour in the region of φ ~ 40-90° phase angle.

The adherence of the antisolar model with the detected Starlink photometry shows evidence that the solar panels are largely Sun-pointing during their operation. This assumption will be further extended when modelling the dayside photometric behaviour as it is likely that the constellation continues its Sun pointing behaviour on either side of Earth's terminator.

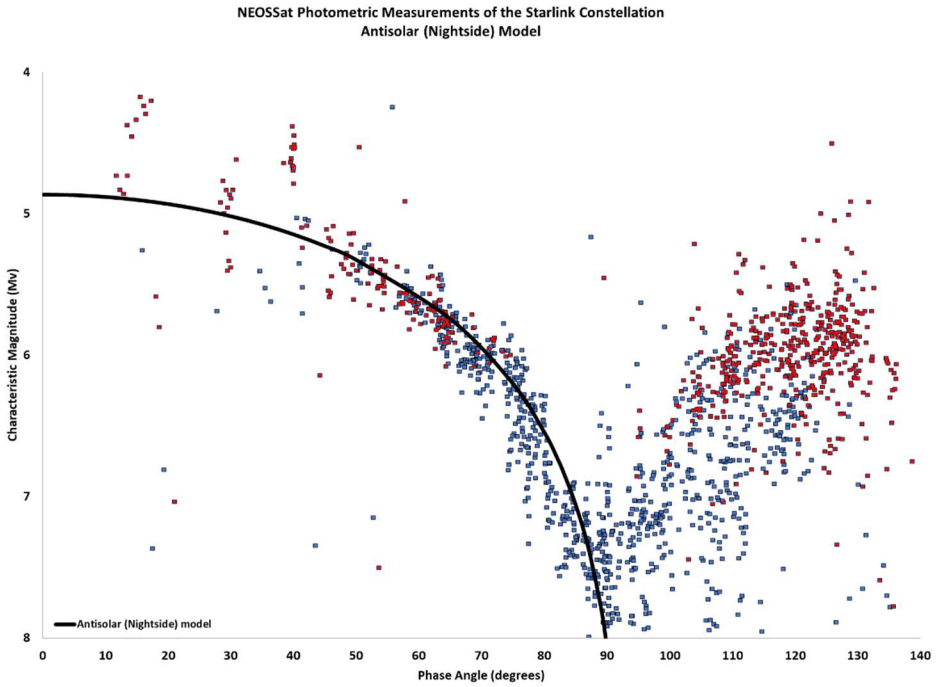

Figure 10: Antisolar Starlink photometric model using a flat plate solar panel and spherical bus for phase angles less than 90 degrees

Dayside Model: Figure 10 shows that for φ greater than 90 degrees there is much more variability in the detected photometry. During high phase angle (dayside) observations, a Starlink satellite is generally illuminated by sunlight back reflected from the Earth and subsequently detected by NEOSSat. This dayside illumination of a Starlink by the Earth is somewhat more complicated. A linearized model, parameterized in terms of the satellite's altitude, *h,* is presented here to account for the Earth's contribution to a Starlink's illumination over Earth's dayside.

This formulation makes use of the relative horizon that a Starlink satellite "sees" of the Earth's surface. This hemispheric surface is approximated as a flat disk despite its actual curved shape (see Figure 11). The

nondimensionalized ratio of the satellite's altitude, h, to the Earth radius $R_\oplus$ is parameterized as $H = h/R_\oplus$. The trigonometric expressions for the Earth's interior angle ϕ to a Starlink's local Earth horizon is then cast in terms of H.

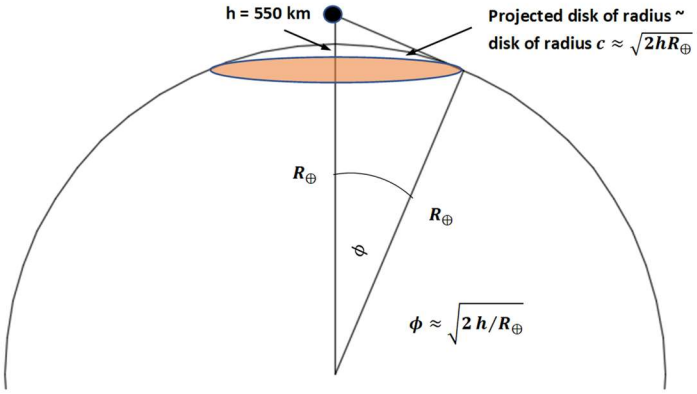

Figure 11: Flat disk approximation of the sector of Earth seen by a LEO satellite

The sunlight reflected from the illuminated patch of Earth extending from the terminator to a Starlink's sub-satellite point quantifies the amount of illumination from the Earth back reflecting onto the solar panel which is pointing toward the Sun (see Figure 12). The parameter x is the linear distance from the Starlink satellite subsatellite point toward the terminator on the virtual (flat) horizon disk shown in Figure 11.

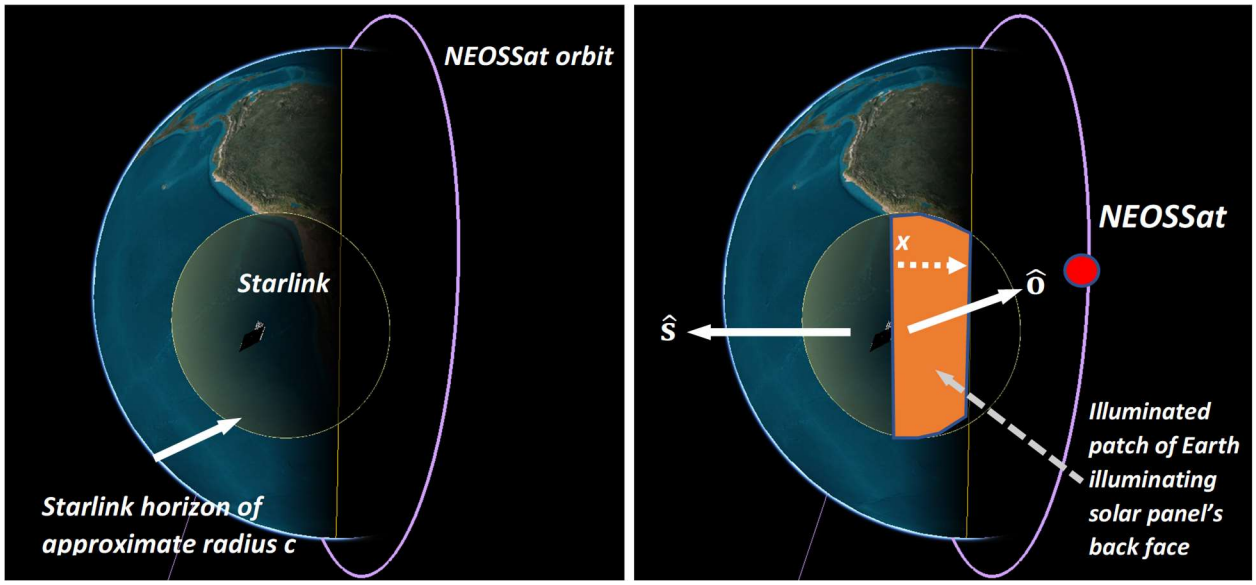

Figure 12: (Left): disk of Earth horizon visible to Starlink satellite with illuminated patch shown. (Right) Observer vector $\hat{o}$ and Sun vector $\hat{s}$ are centered on the Starlink provide the basis for illumination and observation geometry. Note that the phase angle φ is the angle between the observer and Sun vectors.

The nondimensionalized expression for the sunlight reflected from the illuminated flat-disk horizon patch of Earth onto the LEO satellite can be expressed as

$$\frac{F_{\oplus}}{F_{Sun}} \approx \frac{1}{\pi} a_{\oplus} \langle \hat{\mathbf{n}}_{patch} \cdot \hat{\mathbf{s}}_{patch} \rangle \left\{ 2 \int_0^{\sqrt{\frac{2}{H}}} \int_0^{\sqrt{\frac{2}{H} - X^2}} \frac{dXdY}{(1 + X^2 + Y^2)^{3/2}} \right\} \tag{4}$$

where $X = \frac{x}{h}$, $Y = \frac{y}{h}$ and $H = \frac{h}{R_{\oplus}}$. The double integral inside the curly braces is the *view factor Q* of the Earth onto the satellite and is computed numerically as shown in Figure 13.

$$Q = \left\{ 2 \int_0^{\sqrt{\frac{2}{H}}} \int_0^{\sqrt{\frac{2}{H} - X^2}} \frac{dXdY}{(1 + X^2 + Y^2)^{\frac{3}{2}}} \right\} \tag{5}$$

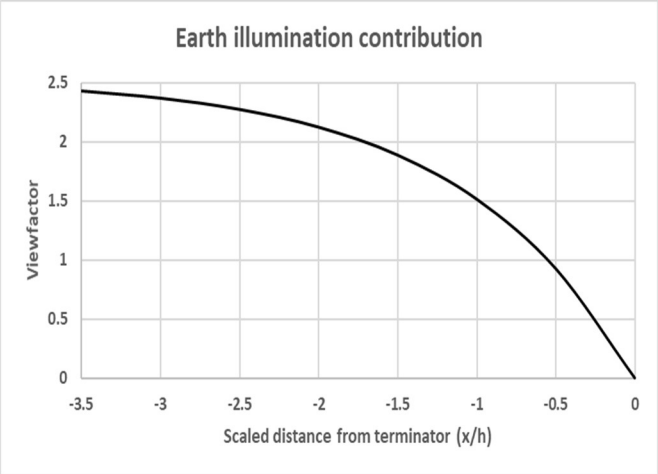

Figure 13: Numerical approximation of the View Factor *Q* representing the fraction of Earth illumination onto a Starlink satellite at nondimensionalized distance from the terminator *X = x/h*

The view factor *Q* can be numerically approximated as $Q \approx 2.54 \cdot \left(1 - e^{X/1.1}\right)$. Here *X = x/h* is the scaled linear distance from a Starlink's sub-satellite point to the Earth's terminator relative to the altitude *h* of the LEO satellite.

The model of the dayside illumination from the Earth on a Starlink satellite can then be cast into magnitudes relative to the Solar flux. The backside of the solar panel is modelled as a flat plate and the bus as a sphere.

$$\begin{aligned} M_{\varphi>90^\circ} = M_{Sun} &- 2.5log_{10}\left(\frac{1}{\pi} \cdot a_{\oplus} \langle \hat{\mathbf{n}}_{patch} \cdot \hat{\mathbf{s}}_{patch} \rangle Q\right) \\ &- 2.5log_{10}\left(\frac{1}{\pi} \cdot \frac{a_{sp_{back}} A_{sp_{back}} \cos(\pi - \varphi)}{R^2}\right) \\ &- 2.5log_{10}\left(\frac{1}{\pi} \cdot \frac{a_{bus} A_{bus} F(\varphi)}{R^2}\right) \end{aligned} \tag{6}$$

where $a_{\oplus}$ is the Earth's albedo, $\hat{\mathbf{n}}_{patch}$ and $\hat{\mathbf{s}}_{patch}$ are the Earth Centred Inertial unit vectors of the satellite position vector and Sun vector, and *Q* is the view factor depending where the sub-satellite point is positioned relative to the terminator. Note that the solar panel's back side albedo and cross-sectional area is

parameterized in the second log term. The Earth's albedo $a_{\oplus}$ is variable and is known to vary from 0.05 over Earth's oceans to as high as 0.8 over the polar caps. The average value of Earth's albedo is taken to be 0.3 [5].

Recognizing that the Earth creates a varying amount illumination on a Starlink satellite and is a function of the satellite's position with respect to the terminator, the angle ξ is used to describe the *depth of terminator* of the subsatellite point from the terminator. $\xi > 0$ represents a subsatellite point on the Earth's dayside with respect to the terminator. In this analysis we do not consider the illumination from the Earth on a Starlink when the satellite is on the nightside. The flat plate model suggests a rapid fall off in brightness while the object traverses over the nightside of the terminator.

$$\xi = \frac{\pi}{2} - \text{acos}(\langle \hat{\mathbf{n}}_{patch} \cdot \hat{\mathbf{s}}_{patch} \rangle) \quad \text{for } \langle \hat{\mathbf{n}}_{patch} \cdot \hat{\mathbf{s}}_{patch} \rangle > 0$$
$$\text{where } \xi \approx \frac{x}{R_{\oplus}} \tag{7}$$

Figure 14 shows the combined nightside and dayside photometric models for various depth of terminator angle ξ overlayed on the range normalized photometry collected by *NEOSSat*. The depth of terminator appears to envelope the extrema of variability in Starlink photometry at higher phase angles. The backside albedo of a Starlink's main solar panel, after model adjustment is estimated to be approximately 0.3. As this is a free fitting parameter, we use the envelopes for various ξ on the detected photometry to estimate its value.

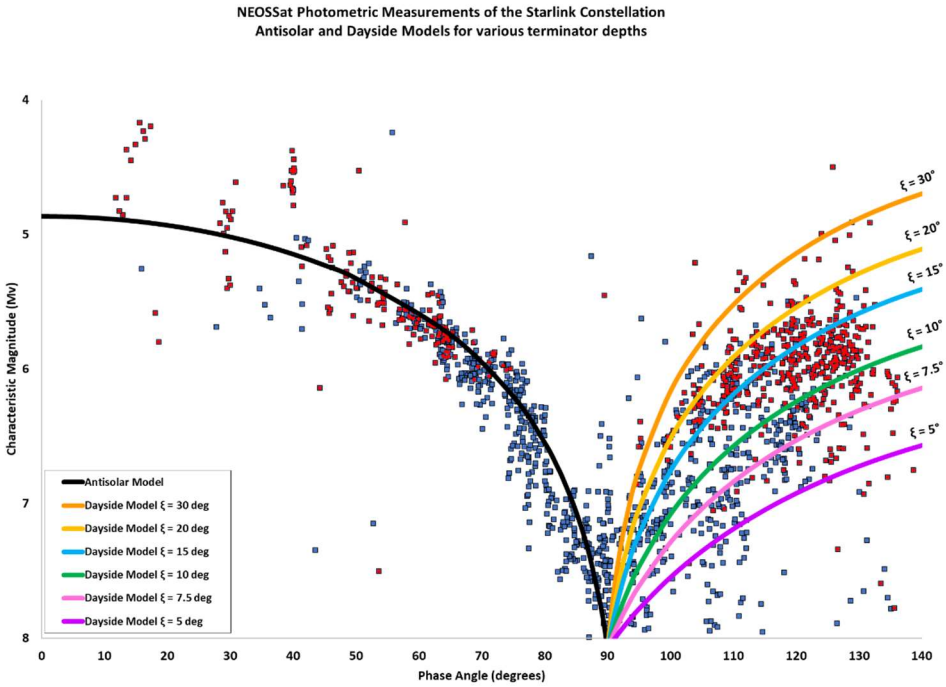

Figure 14: Nightside and Dayside modelling of a Starlink Constellation for various depths of Terminator ξ

Some of the variability seen on the dayside (φ >90°) in Figure 14 may be due to variations in Earth's albedo which was assumed to average $a_{\oplus}$= 0.3 in this analysis. Other modelling improvements which should be considered for future analysis is to better estimate the view factor of the spherical bus as illuminated by the Earth, or model the bus as a small prismatic rectangle which is more consistent with its believed shape.

Key photometric findings. The following estimates for the diffusely reflecting portions of the Starlink satellites are:

- The Sun-facing side of the Starlink satellite main solar panel appears to have a diffuse albedo-area product $a_{sp}A_{sp}$ of approximately 0.6 m^2.
- The backside of the Starlink main solar panel appears to have a diffuse albedo-area product $a_{sp_{back}}A_{sp_{back}}$ of 9 m^2.
- The model of a Starlink bus, while simplified as a sphere in this model, appears to have an albedo-area product of approximately 0.18 m^2.

Comparison to ground-based observations: Starlink satellites have been observed from the ground and are described to range from M_v 3.2 to 7.5 [6]. An astronomer at the University of Maryland collected 830 observations from multiple different sources and determined an average M_v of 5.93 ± 0.02 [7]. The range normalized photometry of the Starlink constellation measured by NEOSSat, not including saturated measurements, resulted in an average M_v of 6.75 ± 0.77. This is nearly a full magnitude lower than current ground measurements, mainly attributed to the large number of satellites observed at lower relative phase angles with lower overall detected magnitudes. These space-based measurements varied from as bright as M_v 3.44 to as dim as M_v 9.96

***Darksat* and *Visorsat* Comparison:** *NEOSSat* space-based measurements included 32 observations of Starlink-1130 also known as *Darksat* (M_v of 6.77 ± 1.19) and 21 observations of Starlink-1436, also known as the first *Visorsat* (M_v of 6.72 ± 1.72). Measurements on these objects, shown in Figure 15, largely follow the lopsided V-shaped trend of the other Starlink satellites. Some lower magnitudes were detected moving outwards in both directions from ~90 degrees phase angle.

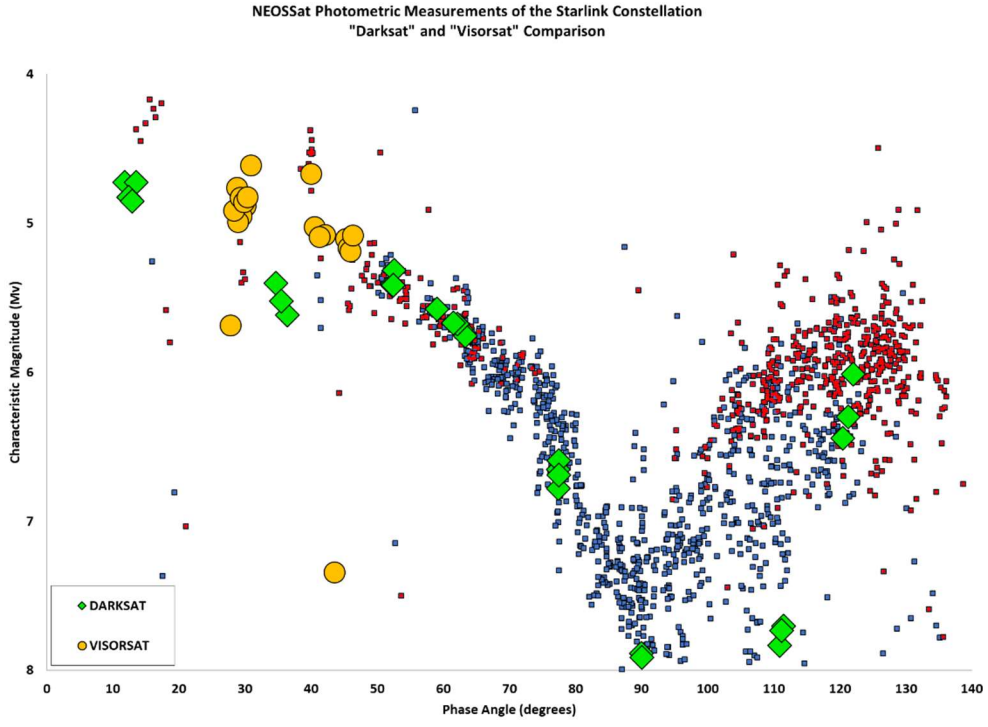

Figure 15: Range normalized photometry of Starlink-1130 and Starlink-1436 vs phase angle

Measurements of *Darksat* typically followed the overall trend for detected magnitude vs. phase angle and its average magnitude was consistent with the overall Starlink measurements (within 0.02 magnitudes), but with a slightly higher standard deviation. The average brightness for *Visorsat* was virtually the same as the overall average Starlink brightness as well (within 0.03). However, the sample size for both *Darksat* and *Visorsat* (after eliminating saturated measurements) was not significant enough for photometric comparison. Overall, it was found that the photometric behaviour for *Darksat* and *Visorsat* appears very similar to all other Starlink satellites when observed from a space-based vantage point. This was anticipated as it is believed that the surface reflectivity modifications on both *Darksat* and *Visorsat* affect the nadir-facing portion of their buses. As *NEOSSat* observes the constellation from above, it primarily observes the Starlink's main solar array which is unaffected by changes in reflectivity on the nadir face of the bus.

CONCLUSION

NEOSSat performed space-based photometric observations of the Starlink satellite constellation from orbit using *NEOSSat's* LEO nodal encounter approach. It was found that the Starlink satellites were easier to observe during their quiescent, non-manoeuvring state such that TLEs can be used to plan observations. Observations attempted during a Starlink satellite's orbital raising phase were not successful.

Photometric measurements were compiled on 247 Starlink satellites in the constellation. A notable fraction of the measured population showed NEOSSat detector saturation suggesting that these Starlinks were likely brighter than reported in this dataset. However, the overall photometric trend of the constellation was preserved for a large fraction of the population. It was found that the constellation's current, range normalized average magnitude is 6.75 over a variety of space-based observing geometries. Range normalized observations revealed a V-shaped photometric behavior in phase angle with the Starlink's faintest magnitude (M_v 8) occurring at 90° phase angle. A first order model to predict the Starlink satellites' expected photometry is consistent with the measurements obtained by *NEOSSat* under both night side and dayside illumination conditions. Measurements taken on *Darksat* and *Visorsat* revealed that their darkening treatments are ineffective when viewed from space. It is believed that these reflectivity treatments principally affect the nadir face of the Starlink satellite bus whereas *NEOSSat* observes the Starlink satellites' main solar array. These photometric results are preliminary and cannot address the effectiveness of darkening methods employed by SpaceX to decrease ground-observed observed brightness of the Starlink satellites. These measurements provide good insight into the photometric behaviour of the Starlink satellites' main solar array and bus behaviour as observed from space which may compliment other ground based studies on this constellation's phenomenology.

When the Starlink satellites are over the dark limb of the Earth, a simple flat-plate model for the Starlink main solar array works well based on the assumption that the solar panels are fully Sun pointing. The close adherence of the anti-solar model with the detected Starlink photometry suggests that the Starlink solar panels are primarily Sun-pointing during operation. A first order photometric model of dayside illumination of the Starlink solar panel's backside show results which envelope the observed photometric behaviour depending on the amount of back reflected light from the Earth onto the back of the Starlink solar panel. Recommended modelling improvements for this analysis include satellite geometry and reflective properties refinement.

This investigation revealed several complexities in tracking large LEO constellations including limitations observing strategy limitations for LEO-to-LEO imaging. As mega-constellations proliferate, this insight will be useful to help ensure an elevated level of Space Situational Awareness, achieve positive control over space objects for collision avoidance, and aid ground-based astronomy of the celestial sphere.

ACKNOWLEDGEMENTS

The authors wish to acknowledge the Canadian Space Agency in their NEOSSat mission operations role and the Royal Canadian Air Force - Director General Air and Space for their support of this work.

REFERENCES

[1] Letzter, Rafi. "Here's Why Astronomers Are So Worried About SpaceX's Planned 'Megaconstellation'." Space.com, Space, 2 June 2019, www.space.com/spacex-astronomers-starlink.html.

[2] Space Exploration Holdings, LLC, Request for Modification of the Authorization for the SpaceX NGSO Satellite System, IBFS File No. SAT−MOD−20181108−00083, filed November 8, 2019 (SpaceX Modification Application).

[3] Scott, R.L., Thorsteinson, S., "Key Findings from the NEOSSat Space-Based SSA Microsatellite Mission" ", AMOS Technical Conference 2018, Maui, HI, (2018).

[4] Celetrak.com, https://celestrak.com/NORAD/elements/supplemental/starlink.rms.txt. Accessed 19 Oct 2020.

[5] Cognion, R.L, "Observations and Modelling of GEO Satellites at Large Phase Angles", AMOS Conference 2013, Poster Paper, Maui Economic Development Board (2013), https://amostech.com/TechnicalPapers/2013/POSTER/COGNION.pdf, accessed 8 Oct 2020.

[6] Hainaut, Olivier R., and Andrew P. Williams. "Impact of Satellite Constellations on Astronomical Observations with ESO Telescopes in the Visible and Infrared Domains." Astronomy & Astrophysics, vol. 636, 2020, doi:10.1051/0004-6361/202037501.

[7] Mallama, Anthony. "Starlink Satellite Brightness Before "Visorsat"." ArXiv.org, 15 June 2020, arxiv.org/abs/2006.08422.

Uncited references

[8] Large Synoptic Survey Telescope. "Vera C. Rubin Observatory – Impact of Satellite Constellations." Vera C. Rubin Observatory – Impact of Satellite Constellations, LSST Corporation, 4 Mar. 2020, www.lsst.org/content/lsst-statement-regarding-increased-deployment-satellite-constellations.

[9] Mann, Adam. "Starlink: SpaceX's Satellite Internet Project." Space.com, Space, 17 Jan. 2020, www.space.com/spacex-starlink-satellites.html.

[10] Space-track.org, Joint Space Operations center, https:www.space-track.org, accessed 23 Mar 2018.

[11] SpaceXchannel. "Starlink Mission." YouTube, www.youtube.com/user/spacexchannel, accessed 2 Sept 2020.